Ship Detection using Linear and Circular Range-Compressed Airborne Radar Data

Sushil Kumar Joshi, Stefan V. Baumgartner
Microwaves and Radar Institute, German Aerospace Center (DLR), Oberpfaffenhofen, Germany

Abstract

In the paper a novel real-time capable ship detection methodology for range-compressed (RC) airborne radar data is proposed. Ships are detected in the range-Doppler domain. The primary advantage of using range-Doppler domain is that ships moving with certain line-of-sight velocity are shifted to the exo-clutter region, thus improving their detection capability. Detection threshold is computed using constant false alarm rate (CFAR) based sea clutter models. Robust estimation of the detection threshold requires an accurate description of the background ocean training data. In the paper, a novel approach to extract reliable ocean training samples is discussed. In addition, different sea clutter models are investigated and compared to choose suitable models for the data. Real linearly and circularly acquired single-channel RC data from DLR's F-SAR system are used to verify the proposed methodology.

1. Introduction

Real-time capable ship detection methods are crucial for monitoring several maritime threats like illegal fishing, migrant and terrorist boats. Currently state-of-the art methods based on automatic identification systems (AIS) and ground radars are used for this task. However, many small ships aren't equipped with AIS transponders and the ground radars suffer from limited visibility [1]. To overcome these limitations, space and airborne radars are desirable choices. One distinguishing feature of airborne radars is their flexibility to collect data with very high resolution and with shorter revisit and longer observation times.

One of the popular ways to address the ship detection problem using radar sensors is based on CFAR (constant false alarm rate). In CFAR, suitable distribution functions are used to model the background ocean data to derive the target detection threshold. However, state-of-the-art CFAR algorithms make use of fully focused radar images to compute such thresholds [2]. Generating these images need extra efforts in terms of processing hardware. Therefore, in this paper we investigate the potential of range-compressed (RC) airborne radar data for ship detection [3]. Targets are detected in the range-Doppler domain of RC data. The primary advantage of using range-Doppler domain is that ships, even with low radar cross section moving with certain line-of-sight velocity are shifted out of the clutter region, where then a detection is possible.

The accuracy of the target detection threshold strongly depends on the proper selection of the ocean training data [4]. Therefore, in the paper we propose an automatic training data extraction method to accurately model the background sea clutter, which then gives a valid detection threshold.

Undoubtedly, the K-distribution is a popular CFAR based distribution function used for target detection. However in practice, even with reliable training data, the performance of the distribution function strongly degrades [5]. This is due to the presence of "discrete sea-spikes", particularly at finer resolutions where the higher backscattered intensity from the spikes extend the tail of the distribution. Therefore, in the paper we compare several alternative models to the K-distribution to select the best models for the airborne radar data. Real linearly and circularly acquired X- and L-band from DLR's F-SAR data [6] are used to verify the robustness of the proposed method.

2. Target detection in range-Doppler

Ships are detected in the range-Doppler domain. A ship moving with certain line-of-sight velocity in time domain is shifted to the exo-clutter region in Doppler domain. An example is shown in **Figure 1**.

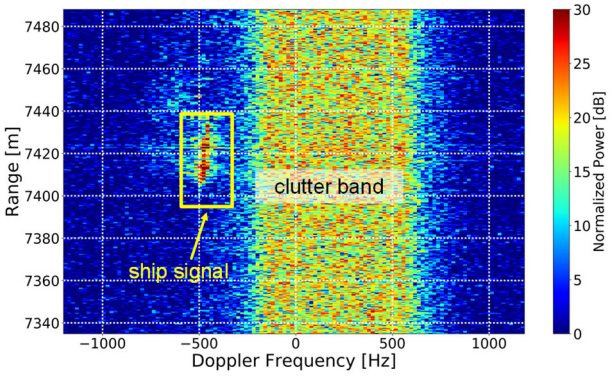

Figure 1 Range-Doppler image of real X-band RC F-SAR data containing 128 azimuth and 512 range samples. The clutter with a bandwidth of around 800 Hz and a ship appearing at -500 Hz (out of the clutter band) are clearly visible (yellow box).

As shown in **Figure 1**, when the moving ship is shifted out of the clutter bandwidth or if the target signal to clutter and noise ratio (SCNR) is high enough, a detection is possible. To compute a CFAR based detection threshold in Doppler domain, reliable ocean training samples are required. In the next section, we show a procedure for extracting ocean training data in Doppler domain for CFAR based target detection threshold computation.

2.1 Training data

Appropriate training samples are crucial to correctly estimate the ocean statistics. Accurate estimation of ocean-only statistics computes a bias-free target detection threshold. However, it is often observed that the data within the region of interest (ROI) is contaminated by bright targets and sea spikes. An example is shown in **Figure 2**.

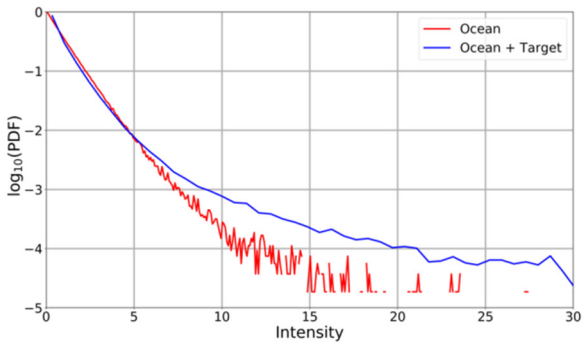

Figure 2 Logarithmic plot of the PDFs (probability density function) of the ocean only (red) and ocean with a ship signal and sea spikes (blue) in time domain.

As shown in the figure, unwanted high target peaks bias the original ocean clutter (blue curve in **Figure 2**). Therefore, they must be pre-detected and cancelled in order to extract target free training data. Several approaches were proposed in the past, like order-statistics CFAR and trimmed CFAR. However, these approaches fail in highly heterogeneous scenarios [7]. Therefore, in the paper we propose a novel target pre-detection method in time-domain which has real time capability if well implemented.
Target pre-detection method starts with the extraction of RC radar data spanning over certain azimuth samples and range bins. An average amplitude profile is then computed by incoherently summing the data along the coherent processing intervals (CPI). If r is the range and $A(r)$ is the average amplitude profile, then the adaptive range-varying threshold is computed by

$$\eta_{pre}(r) = \tilde{A}(r) + f.SG\big(\sigma(r)\big) \qquad (1)$$

where $\tilde{A}(r)$ is the 1-D moving median of $A(r)$, $f > 1$ is a decision criteria to set the uncertainty in the pre-detection threshold, and SG is the Savitzky–Golay filter [8]. The SG filter performs a moving polynomial fit to the data to further reduce the noise level. The standard deviation $\sigma(r)$ in (1) is computed using the following

$$\sigma(r) = k.MAD(r) \qquad (2)$$

where $k \approx 1.4826$ representing the 0.75 quantile of the standard Gaussian distribution. The term $MAD(r)$ is called the median absolute deviation. MAD is a more robust estimator to measure the statistical dispersion and it is found more resilient to the outliers present in the data.

Computing a range-varying threshold is important because the received radar backscatter is range and incidence angle dependent. An example is shown in **Figure 3**.
These values are set based on the expected maximum ship length in slant range direction ($\approx$ 200 m) and the range sample spacing ($\approx$ 0.3 m). However, these values are data-dependent and should be chosen wisely.

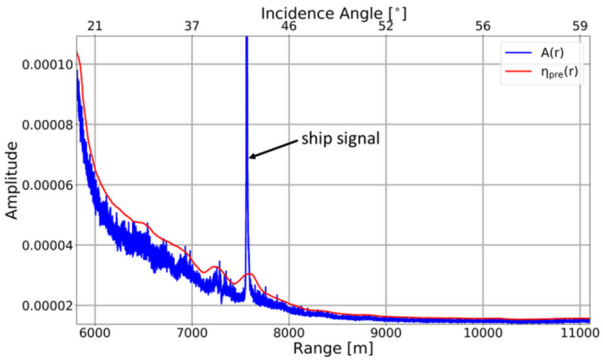

Figure 3 Average amplitude profile $A(r)$ (blue) with range dependent pre-detection threshold $\eta_{\mathrm{pre}}(r)$ (red) computed for real RC X-band F-SAR radar data. A high target peak (= ship) is present at a range of approximately 7500 m.

With the proposed target pre-detection algorithm running in time domain, "target-free" clean training samples are extracted. These data are transformed to Doppler domain where a CFAR threshold can be computed using standard sea clutter models. However, in Doppler domain the training sample amplitude now varies along the Doppler frequency (cf. **Figure 4(a)**). In order to derive a single CFAR threshold, the clutter-plus-noise power is normalized to 0 dB [9]. An example of clutter normalization for a real F-SAR airborne radar data is shown in **Figure 4(b)**.

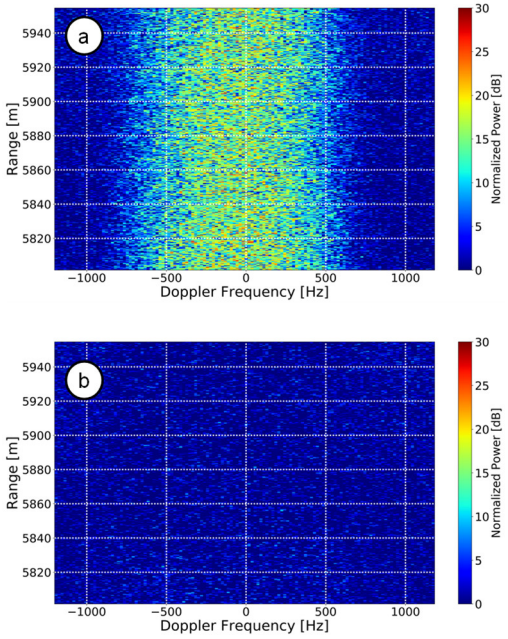

Figure 4 Range-Doppler image (a) before and (b) after clutter normalization.

After normalizing the clutter in **Figure 4(a)** to noise level, the training data is now ready for computing the ocean statistics and subsequently a single CFAR based target detection threshold (cf. **Figure 4(b)**).
Note here that since the ocean surface is constantly in motion and the atmospheric disturbances cause variations in the aircraft's Euler angles (roll, pitch and yaw), the training data (or the detection threshold) needs to be updated along range and azimuth direction. The training data within the moving window contains 128 azimuth and 512 range samples.

2.2 Sea clutter models

One of the most widely accepted sea clutter models to estimate the ocean statistics is the K-distribution. It is a parametric model described in terms of the Rayleigh speckle fluctuations modulated by the gamma distributed texture. Although being a popular model, for a higher incidence angle range (e.g., 10°-50°) and finer resolution data, the real statistics are not always K-distributed. The presence of a non-Bragg scattering component in the ocean surface, better known as discrete sea spikes, is the main reason why the K-distribution fit fails even when the thermal noise is taken into account. Therefore in the paper, we have studied and compared several other sea clutter models to choose suitable models for the investigated F-SAR data. **Table 1** summarizes various sea clutter models with their unknown parameters and methods used to estimate these parameters.

Table 1 Brief description of different sea clutter models used for the airborne radar data.

Sea clutter model	Unknown parameters	Methods
K-distribution [4]	Shape (v, also known as *texture*) and scale, number of looks (L)	Non-linear least square fit (NLLSQ), Method of moments (MoM) (V- and X-statistic)
Chi-square [5]	Standard deviation (σ), L	NLLSQ
Tri-modal discrete texture model [11]	Discrete texture intensity levels and their corresponding relative weightings, L	NLLSQ
K-Rayleigh [10]	Shape (v_r), scale and noise	MoM

Unknown parameters of the K-distribution are estimated using three different methods (cf. **Table 1**). The Chi-square distribution is preferred when the parameters estimated by the K-distribution are negative. The 3MD model is based on the idea of the statistical modeling of the sea clutter in discrete form. The K-Rayleigh distribution function is preferred when the sea clutter suffers from discrete sea spikes [3], [10], [11]. If $f(I)$ is the distribution function, then the probability of false alarm (PFA) can be written as

$$P_{\text{fa}} = \int_{\eta}^{\infty} f(I)\, dI. \tag{3}$$

After setting the PFA to a constant value, the detection threshold η can be computed using (3). In experimental result section, we provide some comparison results of different sea clutter models and detection results of real moving ships in the data. The investigated radar data for ship detection were acquired linearly and circularly during a dedicated experiment carried out with a controlled German federal police ship during an F-SAR campaign in the North Sea in 2016 [12].

3. Experimental results

To better understand the behavior of the ocean clutter, the data is partitioned into three regions: (a) near range (15°-30° incidence angle), (b) mid range (30°-50°) and (c) far range (> 50°). This is because the radar-based ocean backscatter significantly changes along range (cf. **Figure 3**). Different sea clutter statistics are fitted to the linearly acquired RC airborne radar data and the results are shown in **Figure 5**.

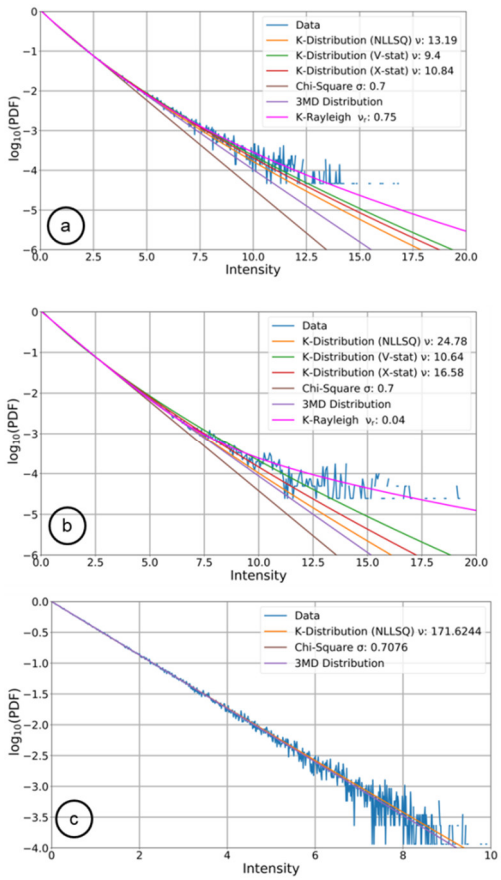

Figure 5 Logarithmic PDFs in Doppler domain using different distribution functions plotted for (a) near (b) mid and (c) far range of linearly acquired X-band F-SAR data. The estimated parameters corresponding to different distribution functions are shown in the legends of the plots, apart from the 3MD model since a listing of its parameters needs too much space.

From the results shown in **Figure 5(a)** and **(b)** it is obvious that the K-Rayleigh outperforms other sea clutter models by fitting well with the data in near and mid-range. However, in far range only the K-distribution parameters estimated using the NLLSQ method, the chi-square and the

3MD model fit well to the data (cf. **Figure 5(c)**). This is due to the long range and shallow incidence angle of the acquired data so that the clutter power in far range is comparable to the noise power [10], as shown by the green curve in **Figure 6**.

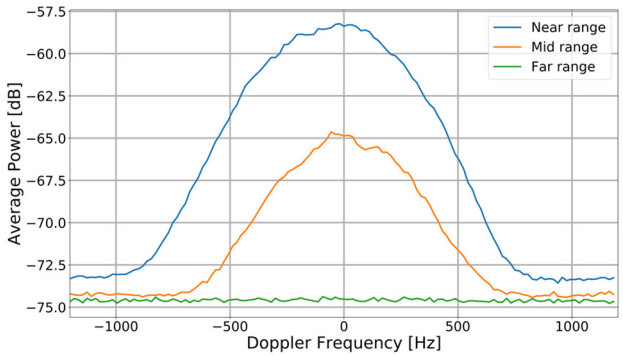

Figure 6 Average Doppler spectrum of the data estimated in near, mid and far range. Azimuth ambiguities cause a variation in the average power in the noise region of the spectrum.

From **Figure 6** it is observed that in far range the clutter power is comparable to the noise power. K-distribution based on NLLSQ estimates a very high texture value (cf. **Figure 5(c)** where $\nu \approx 171$) in far range, implying Rayleigh distributed statistics.
Additionally, we have also investigated two important metrics to compare the performance of the chosen sea clutter models, namely: false alarm rate ratio (FARR) and threshold error. The FARR is estimated as the ratio between the estimated and the set false alarm rate. The set false alarm rate is 10^{-6} and in an optimum case, FARR should be 1. **Table 2** shows the FARR computed in near, mid and far range for different sea clutter models.

Table 2 FARR computed for the near, mid and far range of the real F-SAR airborne radar data. The set false alarm rate is 10^{-6}. The values in bold are closest to the optimum and desired value of FARR=1.

Distribution functions	Near range FARR	Mid-range FARR	Far range FARR
K-NLLSQ	80.5	112.1	3.08
K-Vstat	35.1	57.1	-
K-Xstat	56.9	86.8	-
Chi-square	277.4	242.9	2.43
3MD	149.2	135.9	**1.56**
K-Rayleigh	**1.31**	**1.68**	-

From the table it is clear that the K-Rayleigh performs better than other models in near and mid range. However, in far range, the 3MD model gives the best performance. FARR cannot be computed for V-statistic, X-statistic and K-Rayleigh in far range. The reason can again be explained in terms of low clutter-to-noise ratio (CNR) and the Rayleigh distributed characteristics (cf. **Figure 6**).

The threshold error is calculated as the absolute difference between the thresholds estimated from the data CCDF (complementary cumulative distribution function) and the model CCDF at a certain CCDF value in the tail region of the histogram. The threshold error is computed in the tail region because of two reasons: bright ship target signals lie mostly in that region and the tail region is the region where most of the mismatch between reality and models occurs. Threshold error computation is illustrated in **Figure 7**.

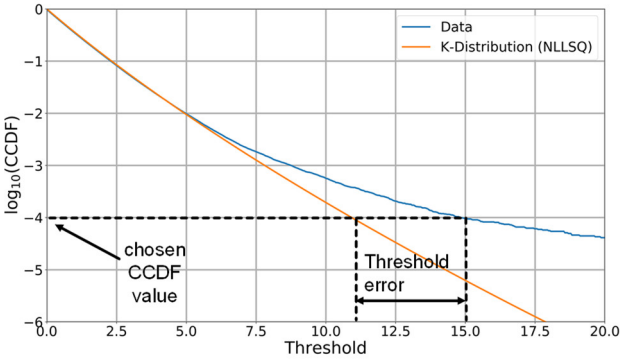

Figure 7 Threshold error computation using logarithmic CCDF plots from the real data and the K-Distribution NLLSQ method plotted against the threshold. Threshold error and the chosen CCDF value are marked in the figure.

In our case the CCDF value chosen to compute the threshold error is 10^{-4} and the results are shown in **Table 3**.

Table 3 Estimated threshold errors in log scale for different clutter models at near, mid and far ranges.

Clutter models	Near range CCDF	Mid range CCDF	Far range CCDF
	10^{-4}	10^{-4}	10^{-4}
K-NLLSQ	6.89	6.02	-5.86
K-Vstat	5.19	4.60	-
K-Xstat	6.19	5.49	-
Chi-square	9.70	7.73	**-11.65**
3MD	8.94	6.94	-10.86
K-Rayleigh	**-6.68**	**2.27**	-

From **Table 3** it can be inferred that the K-Rayleigh gives the minimum errors in near and mid range and the chi-square model in far range. NLLSQ-based K-distribution and the 3MD model also give relatively good results in far range.
Based on these analyses, it can be concluded that for near and mid ranges, the K-Rayleigh distribution function is the best choice, whereas for the far range, the 3MD model, the chi-square or the K-distribution NLLSQ is preferred. This recommendation is at least valid for the RC X-band HH polarized F-SAR data used for the investigations and the current sea state conditions during the data acquisitions.
The binary ship detection map of the linearly acquired real F-SAR RC data is shown in **Figure 8(b)**. The detection

threshold is estimated based on a constant false alarm rate of 10^{-6}.

In **Figure 8**, the detected ship signal is clearly visible both in the data and in the binary detection map. The proposed algorithm is also applied onto the real circularly acquired L-band HH polarized data. The detection results are shown in **Figure 9**.

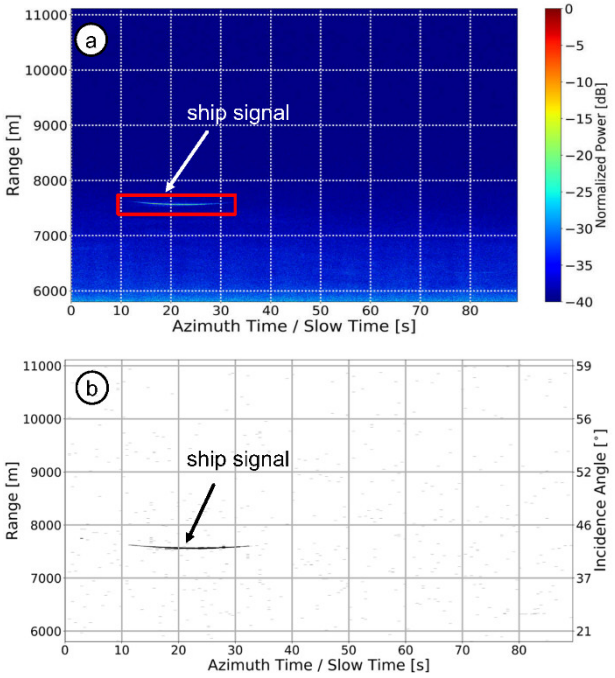

Figure 8 (a) Linearly acquired real single-channel HH polarized RC X-band radar data. (b) Corresponding binary detection map shown in time-domain after applying CFAR based ship detection in range–Doppler domain.

4. Conclusion

A ship detection methodology based on CFAR for range-compressed airborne radar data is proposed. Target pre-detection and cancellation in time domain and clutter normalization in Doppler domain extract reliable training data. The training data are used to model the sea clutter for computing a reliable target detection threshold. After investigating various sea clutter models, we conclude that the K-distribution cannot be used at near (15°-30° incidence angle) and mid ranges (30°-50°). The chi-square and the 3MD model lead to extremely high false alarm rate errors and threshold errors in near and mid ranges. On the contrary, the K-Rayleigh distribution is the best choice in near (15°-30° incidence angle) and mid ranges (30°-50°). In far range (> 50° incidence angle) which is mostly dominated by the thermal noise, the 3MD model, the chi-square or the NLLSQ based K-distribution can be used. We would also like to point out that the data acquisition during the F-SAR flights lasted only a few hours. Therefore, it can be expected that the sea state has not changed significantly. More radar data at different sea states are recommended for more sophisticated investigations.

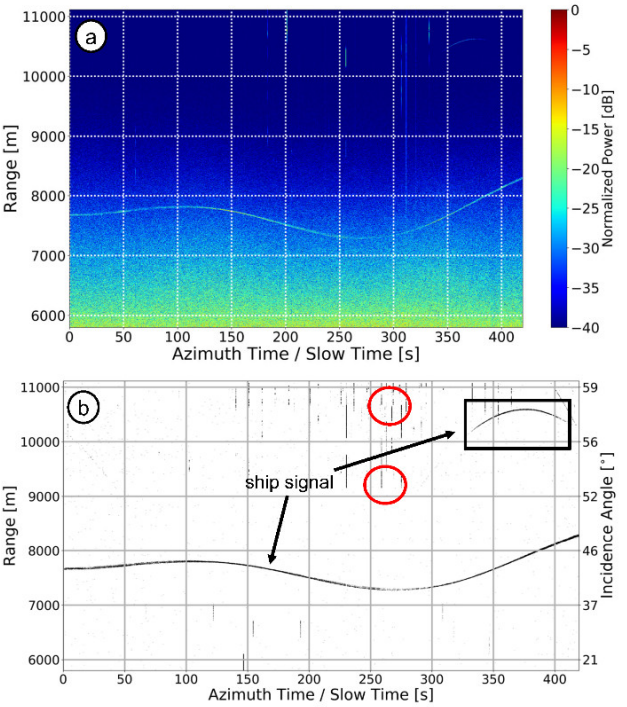

Figure 9 (a) Real single-channel HH polarized RC L-band radar data using circular flight track. (b) Binary detection map shown in time-domain after applying CFAR based ship detection in range–Doppler domain. The detections marked by the red circles are due to the interfering signals from a ground surveillance radar located close to the test site.

References

[1] F. Te Hennepe, R. Rinaldo, A. Ginesi, C. Tobehn, M. Wieser, Ø. Olsen, Ø. Helleren, R. Challamel and F. Storesund, "Space-based detection of AIS signals: Results of a feasibility study into an operational space-based AIS system," in *ASMS/SPSC 2010: 2010 5th Advanced Satellite Multimedia Systems Conference and the 11th Signal Processing for Space Communications Workshop*, 2010, pp. 17–24.

[2] S. Brusch, S. Lehner, T. Fritz, M. Soccorsi, A. Soloviev, and B. Van Schie, "Ship surveillance with TerraSAR-X," *IEEE Trans. Geosci. Remote Sens.*, vol. 49, no. 3, pp. 1092–1103, 2011.

[3] S. K. Joshi, S. V Baumgartner, A. B. C. Silva, and G. Krieger, "Range-Doppler Based CFAR Ship Detection with Automatic Training Data Selection," *Remote Sens.*, vol. 11, no. 11, p. 1270/1-1270/39, 2019.

[4] K. D. Ward, R. J. A. Tough, and S. Watts, "Sea clutter: Scattering, the K distribution and radar performance," *Waves in Random and Complex Media*, vol. 17, no. 2, pp. 233–234, 2007.

[5] D. J. Crisp, “The State-of-the-Art in Ship Detection in Synthetic Aperture Radar Imagery,” *Inf. Sci. (Ny).*, no. DSTO-RR-0272, p. 115, 2004.

[6] A. Reigber, R. Horn, A. Nottensteiner, P. Prats, R. Scheiber, K. Bethke and S. V. Baumgartner, “Current status of DLR’s new F-SAR sensor,” in *EUSAR*, 2010, pp. 1078–1081.

[7] J. T. Rickard and G. M. Dillard, “Adaptive Detection Algorithms for Multiple-Target Situations,” *IEEE Trans. Aerosp. Electron. Syst.*, vol. AES-13, no. 4, pp. 338–343, 1977.

[8] R. W. Schafer, “What is a savitzky-golay filter?,” *IEEE Signal Process. Mag.*, vol. 28, no. 4, pp. 111–117, 2011.

[9] L. Rosenberg and S. Watts, “Model based coherent detection in medium grazing angle sea-clutter,” in *2016 IEEE Radar Conference, RadarConf 2016*, 2016.

[10] L. Rosenberg, S. Watts, and S. Bocquet, “Application of the K+Rayleigh distribution to high grazing angle sea-clutter,” in *2014 International Radar Conference, Radar 2014*, 2014.

[11] C. H. Gierull and I. Sikaneta, “A Compound-Plus-Noise Model for Improved Vessel Detection in Non-Gaussian SAR Imagery,” *IEEE Trans. Geosci. Remote Sens.*, vol. 56, no. 3, pp. 1444–1453, 2018.

[12] S. V Baumgartner, “Linear and Circular ISAR Imaging of Ships Using DLR ’ s Airborne Sensor F-SAR,” in *IET Radar*, 2017.